The interplay of local electron correlations and ultrafast spin dynamics in fcc Ni: Supplementary material

Tobias Lojewski,[1] Mohamed F. Elhanoty,[2] Loïc Le Guyader,[3] Oscar Grånäs,[2] Naman Agarwal,[3,*] Christine Boeglin,[4] Robert Carley,[3] Andrea Castoldi,[5,6] Christian David,[7] Carsten Deiter,[3] Florian Döring,[7] Robin Y. Engel,[8] Florian Erdinger,[9,†] Hans Fangohr,[3,10,11] Carlo Fiorini,[5,6] Peter Fischer,[9] Natalia Gerasimova,[3] Rafael Gort,[3] Frank de Groot,[12] Karsten Hansen,[8] Steffen Hauf,[3] David Hickin,[3] Manuel Izquierdo,[3] Benjamin E. Van Kuiken,[3] Yaroslav Kvashnin,[2] Charles-Henri Lambert,[13] David Lomidze,[3] Stefano Maffessanti,[8] Laurent Mercadier,[3] Giuseppe Mercurio,[3] Piter S. Miedema,[8] Katharina Ollefs,[1] Matthias Pace,[4] Matteo Porro,[3,14] Javad Rezvani,[15] Benedikt Rösner,[7] Nico Rothenbach,[1] Andrey Samartsev,[3,8] Andreas Scherz,[3] Justina Schlappa,[3] Christian Stamm,[13,16] Martin Teichmann,[3] Patrik Thunström,[2] Monica Turcato,[3] Alexander Yaroslavtsev,[2,3] Jun Zhu,[3] Martin Beye,[8] Heiko Wende,[1] Uwe Bovensiepen,[1] Olle Eriksson,[2] and Andrea Eschenlohr[1,‡]

[1] *Faculty of Physics and Center for Nanointegration Duisburg-Essen (CENIDE), University of Duisburg-Essen, Lotharstr. 1, 47057 Duisburg, Germany*
[2] *Department of Physics and Astronomy, Uppsala University, 75120 Uppsala, Sweden*
[3] *European XFEL, Holzkoppel 4, 22869 Schenefeld, Germany*
[4] *Université de Strasbourg, CNRS, Institut de Physique et Chimie des Matériaux de Strasbourg, UMR 7504, Strasbourg 67000, France*
[5] *Dipartimento di Elettronica, Informazione e Bioingegneria, Politecnico di Milano, 20133 Milano, Italy*
[6] *Istituto Nazionale di Fisica Nucleare, Sez., Milano, 20133 Milano, Italy*
[7] *Paul Scherrer Institute, 5232 Villigen PSI, Switzerland*
[8] *Deutsches Elektronen-Synchrotron DESY, Notkestr. 85, 22607 Hamburg, Germany*
[9] *Institute for Computer Engineering, University of Heidelberg, Im Neuenheimer Feld 368, 69120 Heidelberg, Germany*
[10] *Max-Planck Institute for the Structure and Dynamics of Matter, Luruper Chaussee 175, 22761 Hamburg, Germany*
[11] *University of Southampton, Southampton SO17 1BJ, United Kingdom*
[12] *Materials Chemistry and Catalysis (MCC), Debye Institute for Nanomaterials Science, Utrecht University, Universiteitslaan 99, 3584 CG, Utrecht, The Netherlands*
[13] *Department of Materials, ETH Zurich, 8093 Zurich, Switzerland*
[14] *Department of Molecular Sciences and Nanosystems, Ca' Foscari University of Venice, 30172 Venezia, Italy*
[15] *Laboratori Nazionali di Frascati, INFN, Via Enrico Fermi 54, 00044 Frascati (Roma), Italy*
[16] *Institute for Electric Power Systems, University of Applied Sciences and Arts Northwestern Switzerland, 5210 Windisch, Switzerland*

(Dated: April 24, 2023)

METHODS

In this supplementary material, we detail the steps taken in preparing the samples and analysing the experimental data, provide further detail for the time-dependent density functional theory (TDDFT) calculations, and describe the process of comparing the calculated and measured absorption spectra.

Sample preparation

Polycrystalline fcc Ni film samples were evaporated on a 5×5 array of 200 nm thick Si_3N_4 windows, with the middle window being left uncovered for the reference measurement. They consist of a 20±0.7 nm thick fcc Ni layer, capped by 2 nm MgO. A 100 nm thick Cu layer was deposited on the backside of the window to mitigate heating effects. The samples are polycrystalline and ferromagnetically ordered [1].

Treatment of experimental data

In the measured absorption spectra, we find a linear background, which we attribute to the zone plate, and that leads the excited- and ground-state spectra to diverge over the energy range. We correct this background for both spectra using two linear functions with the same slope of opposite sign, thus leading the two spectra to coincide in the pre- and post-edge regions. Following the correction, the spectra are normalised so that the mean of the pre-edge region corresponds to zero, while the mean in the post-edge region corresponds to one. The measurement of the transient absorption change is then scaled with the same factor obtained from the normalisation of the spectra. This ensures continued agreement between the induced changes observed in the spectra and the evolution of the absorption changes.

We note that in order to exclude any influence of effects resulting from heat build-up in the sample within one x-ray pulse train, only the first six pulses in each train are evaluated in the analysis.

Analysing the induced changes

In order to reproduce the pumped spectrum and pump-induced change, as seen in Fig. 1(b,c) of the main paper, two modifications of the unpumped spectrum are considered, a rigid energy shift and a broadening. This modelling was done with the program Pi [2]. The energy shift is incorporated by calculating an Akima spline of the unpumped spectrum where the energy axis is shifted by ΔE. In contrast, the broadening is included via a convolution of this Akima spline with a Gaussian with the FWHM ω. The two parameters are optimised so that the agreement of the modified Akima spline and the measured pumped spectrum is optimal in the energy range where the induced change is at its maximum (852 - 853.5 eV). By setting one of the parameters, ω or ΔE, to zero, the corresponding modification is also reduced to zero, identifying the individual contribution of the two modifications, as shown in Fig. 1(c) of the main paper.

For the purpose of analysing the transient absorption change at a constant $h\nu = 852.72$ eV, the response function [3] Eq. (S1) is convoluted with a Gaussian of FHWH ω and fitted to the experimental data to obtain the exponential rise τ_{th} and decay time τ_{e-ph}:

$$A_0 + \Theta(t-t_0)\left(A_{th}\cdot\left[1-e^{\frac{-(t-t_0)}{\tau_{th}}}\right]\cdot\left[e^{\frac{-(t-t_0)}{\tau_{e-ph}}}\right] + A_{e-ph}\cdot\left[1-e^{\frac{-(t-t_0)}{\tau_{e-ph}}}\right]\right) \tag{S1}$$

As the response function is obtained in the framework of the two temperature model the two time constants τ_{th} and τ_{e-ph} can be assigned to the internal thermalisation time of the electronic system and the electron-phonon coupling time respectively [3]. Following the convolution the function can be written as:

$$\begin{aligned} &A_0 + e^{-z_1}\cdot(-A_{th}\cdot e^{z_2} + A_{e-ph}\cdot e^{z_1} + \\ &(A_{th}-A_{e-ph})\cdot e^{z_3} - \sqrt{\frac{1}{\omega^2}}\cdot\omega\cdot \\ &(A_{th}\cdot e^{z_1}\cdot erf\left[\frac{2t_0-t}{\omega\sqrt{2}}\right] + (A_{th}-A_{e-ph})\cdot e^{z_3}\cdot \\ &erf\left[\frac{2t_0\tau_{e-ph}+\omega^2-\tau_{e-ph}t}{\omega\tau_{e-ph}\sqrt{2}}\right] - A_{th}\cdot e^{z_2}\cdot \\ &erf\left[\frac{2t_0\tau_{e-ph}\tau_{th}+(\tau_{e-ph}+\tau_{th})\omega^2-\tau_{e-ph}\tau_{th}t}{\omega\tau_{e-ph}\tau_{th}\sqrt{2}}\right])) \\ &/2\omega\sqrt{\frac{1}{\omega^2}} \end{aligned} \tag{S2}$$

with:

$$z_1 = \left(\frac{1}{\tau_{e-ph}}+\frac{1}{\tau_{th}}\right)\cdot t$$

$$z_2 = \frac{(\tau_{e-ph}+\tau_{th})\cdot(4t_0\tau_{e-ph}\tau_{th}+(\tau_{e-ph}+\tau_{th})\cdot\omega^2)}{2\tau_{e-ph}^2\tau_{th}^2}$$

$$z_3 = \frac{4t_0\tau_{e-ph}+\omega^2}{2\tau_{e-ph}^2}+\frac{t}{\tau_{th}}$$

The results are double-checked using two separate programs, one fitting the convoluted form and one where the function is convoluted during the fitting procedure leading to identical fit parameters within the error. The results of fitting the convoluted response function Eq. (S2) can be seen in Fig. 2(b) of the main paper.

TDDFT formalism

The time-dependent Kohn-Sham (TDKS) Hamiltonian can be written as:

$$\left[\frac{1}{2}\left(-i\nabla+\frac{1}{c}\mathbf{A}_{ext}(t)\right)^2 + v_s(\mathbf{r},t) + \frac{1}{2c}\sigma\cdot\mathbf{B}_s(\mathbf{r},t) + \frac{1}{4c^2}\sigma\cdot\left(\nabla v_s(\mathbf{r},t)\times -i\nabla\right)\right]\psi_i(\mathbf{r},t) = \frac{\partial\psi_i(\mathbf{r},t)}{\partial t}, \tag{S3}$$

where c is the speed of light, σ is the Pauli matrix, and $\mathbf{B}_s(\mathbf{r},t)$ is the effective Kohn-Sham (KS) magnetic field ($\mathbf{B}_s(\mathbf{r},t) = \mathbf{B}_{ext}(t) + \mathbf{B}_{XC}(\mathbf{r},t)$, where $\mathbf{B}_{ext}(t)$ is the magnetic field of the external laser pulse and $\mathbf{B}_{XC}(\mathbf{r},t)$ is the exchange-correlation (XC) induced exchange splitting. The last term of Eq. (S3) is the spin-orbit coupling (SOC) term in its generic form, and $\psi_i(\mathbf{r},t)$ is the two component Pauli spinor. The external laser pulse is treated in the dipole approximation with a vector potential $\mathbf{A}_{\mathrm{ext}}(\mathrm{t})$. The atomic units (with

$\hbar = e$ =m=1) are adopted in Eq. (S3).

The KS effective potential, $v_s(\mathbf{r},t)$, is a sum of three terms $v_s(\mathbf{r},t) = v_{ext}(\mathbf{r},t) + v_H(\mathbf{r},t) + v_{xc}(\mathbf{r},t)$, where $v_{ext}(\mathbf{r},t)$ is the external potential, $v_H(\mathbf{r},t)$ is the Hartree potential, and $v_{XC}(\mathbf{r},t)$ is the exchange-correlation (XC) potential.

We note that while the TDDFT calculations accurately describe the non-equilibrium electronic state after optical excitation, they are performed with fixed nuclei and thus apply only to the first $\approx$ 100 fs during which the influence of lattice excitations can be safely neglected [4, 5].

Comparing theoretical calculations and experimental data

To directly compare the experimental and calculated absorption spectra, several steps are taken.

Preparing experimental data

The experimental as well as the absorption spectra calculated from TDDFT and DFT show a varying level of contributions from excitations into the continuum. As such, these contributions have to be corrected in order to compare the data directly. In the case of the measured absorption spectra, the excitations into the continuum are corrected by subtracting a step-function of the form:

$$A_{L3} \cdot \left(\frac{1}{1 + e^{\omega \cdot (E_{L3} - E)}} \right) + A_{L2} \cdot \left(\frac{1}{1 + e^{\beta\omega \cdot (E_{L2} - E)}} \right) \tag{S4}$$

where E_{L3} and E_{L2} determine the energy position of the steps and are chosen corresponding to the maximum of the $L_{3,2}$-edge in the ground-state spectrum. The parameter ω determines the width of the steps, and the additional parameter β is added to account for the additional broadening of the L_2-edge due to the additional L_2L_3V Coster-Kronig decay channel [6]. For the experimental spectra, the parameters A_{L3} and A_{L2} are set to $\frac{2}{3}$ and $\frac{1}{3}$, respectively, according to the branching ratio in nickel [7].

Incorporation of lifetime broadening for theoretical spectra

Furthermore, before the experimental and calculated absorption spectra can be directly compared, the calculated spectra have to be broadened to account for the lifetime broadening effects of the two absorption edges. This is done by convoluting the calculated spectra with a Lorentzian, whose FWHM increases linearly with energy, to consider the energy dependence of the Hedin-Lundqvist self-energy [8]. Here we chose to increase the FWHM of the Lorentzian by 0.1 eV for every eV on the energy scale, with the evolution of the FWHM over the energy range being shown in Fig. S1(bottom). We also consider the increased broadening of the L_2-edge with an increased starting value for the FWHM.

Preparing convoluted theoretical data

Following the convolution, a step-function Eq. (S4) is subtracted, but as the contribution of the excitations into the continuum is not identical in the calculations and the experiment, the parameters A_{L3} and A_{L2} have to be adjusted accordingly. Furthermore, the absolute energy scale of the theoretical calculations does not coincide with the experimentally measured one. As such, E_{L3} and E_{L2} are also adjusted to again correspond to the maximum of the $L_{3,2}$-edge in the ground-state spectrum. To compare

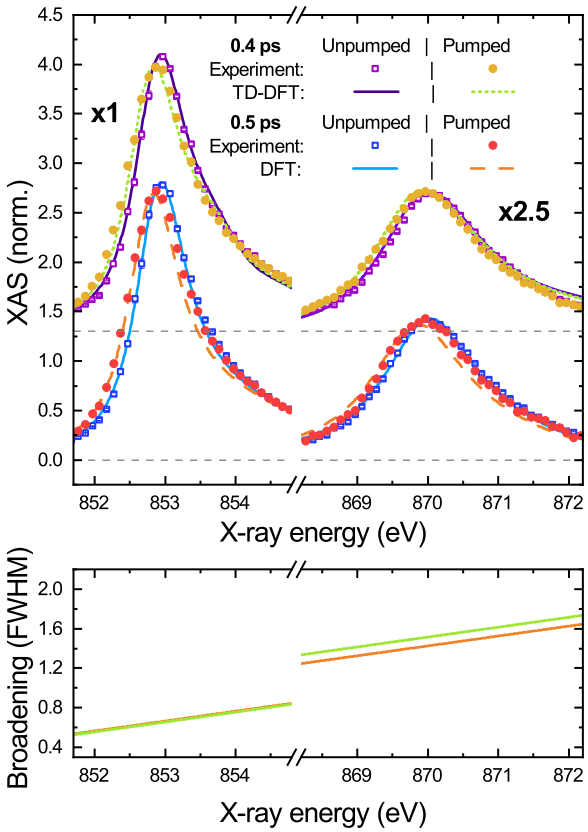

FIG. S1. (top) Ground-state (purple/blue squares) and pumped (yellow/red circles) X-ray absorption spectra at Δt = 0.4 ps and 0.5 ps, respectively, compared with the broadened calculated ground-state (purple/blue line) and excited (green dotted/red dashed line) absorption spectra obtained from TDDFT and DFT. (bottom) Evolution of the FWHM of the Lorentzian used for broadening the calculated absorption spectra from TDDFT (green) and DFT (orange) over the energy range.

the spectra, the energy scale is shifted by ΔE, with the energy scale of the L_2-edge spectrum being shifted by the additional amount ΔE_{L2}. Finally, the spectra are scaled so that the agreement between the calculated and measured ground-state spectrum is good. The parameters for the broadening are determined once in that way for the TDDFT and DFT calculations and then kept identical for all calculations in each data-set. An exemplary broadened ground state and excited spectrum is shown in Fig. S1(top) in comparison with the experimental data.

* present address: Department of Physics and Astronomy (IFA), Aarhus University, NY Munkegade 120, 8000 Aarhus C, Denmark
† present address: EXTOLL GmbH, 68159 Mannheim, Germany
‡ andrea.eschenlohr@uni-due.de

[1] N. Rothenbach, *Femtosecond time-resolved soft X-ray spectroscopy for an element-specific analysis of complex materials*, Ph.D. thesis, University of Duisburg-Essen, Germany (2020).
[2] U. von Hörsten, "Pi," (2023).
[3] N. Del Fatti, C. Voisin, M. Achermann, S. Tzortzakis, D. Christofilos, and F. Vallée, Phys. Rev. B **61**, 16956 (2000).
[4] W. S. Fann, R. Storz, H. W. K. Tom, and J. Bokor, Phys. Rev. B **46**, 13592 (1992).
[5] H.-T. Chang, A. Guggenmos, S. K. Cushing, Y. Cui, N. U. Din, S. R. Acharya, I. J. Porter, U. Kleineberg, V. Turkowski, T. S. Rahman, D. M. Neumark, and S. R. Leone, Phys. Rev. B **103**, 064305 (2021).
[6] S. Iacobucci, M. Sacchi, L. Marassi, V. Marocchi, and G. Stefani, Phys. Rev. B **59**, 9898 (1999).
[7] C. T. Chen, F. Sette, Y. Ma, and S. Modesti, Phys. Rev. B **42**, 7262 (1990).
[8] J. Mustre de Leon, J. J. Rehr, S. I. Zabinsky, and R. C. Albers, Phys. Rev. B **44**, 4146 (1991).